Journal of the Chinese Society of Mechanical Engineers, Vol.47, No.2, pp 175~184 (2026)

Exploring the Role of the Inlet Machining Angle on the Pressure and Flow Characteristics of Microchannels under Slip Flow Conditions

Ayhan Nazmi İlikan*

Keywords：microchannel, slip flow, CFD, machining angle.

ABSTRACT

This study numerically investigates how machining inlet angles affect the pressure drop and hydrodynamic entrance length in microchannels. Two-dimensional CFD simulations were performed under steady conditions with Reynolds (Re) numbers ranging from 1-100 and Knudsen (Kn) numbers of 0.001, 0.01, and 0.1 within the slip flow regime. Air was used as the working fluid, and the Navier–Stokes equations were solved with Maxwell slip boundary conditions. The results show that at constant inlet machining angles and Re values, the pressure drop increased by up to 75% as Kn decreased from 0.1 to 0.001. For all Kn values, the pressure loss increased by an average of 3% at a 15° angle, 10% at 30°, and 25% at 45° compared with that of a straight channel. As Re increased, these values escalated further. The findings suggest that pressure loss tends to increase significantly for inlet angles above 30°, particularly at higher Reynolds numbers; therefore, keeping the angle below this value may be beneficial. Additionally, the entrance length increased with both Re and Kn, with the inlet machining angle affecting it only when the channel length matched the diameter at Re 1 or was 7-8 times the diameter at Re 100. No substantial effect was observed for longer channels. The results aligned well with the literature, supporting the conclusions of the present study.

INTRODUCTION

With advancements in manufacturing technologies, the size of heat exchangers has significantly decreased, reaching microscales. Channels with diameters ranging from 1 μm to 999 μm are now referred to as microchannels (Prakash & Kumar (2015)).

Paper Received January, 2025. Revised May, 2025. Accepted May, 2025. Author for Correspondence: Ayhan Nazmi İlikan.

* *Chief Researcher, Alternative Energy Technologies Department, TUBITAK RUTE, Gebze, Kocaeli, Türkiye*

These channels provide greater efficiency because of their increased heat transfer surface and offer advantages such as being lighter and more cost-effective, requiring less material because of their smaller size. Owing to their high surface-to-volume ratio and enhanced heat and mass transfer capabilities, microchannels have applications in diverse fields, including automotive, aerospace, fuel cell, high-flux electronics cooling, microelectromechanical system (MEMS), biomedical device, and chemical reactor fields. As channel sizes reduce to the microscale, rarefaction effects become significant, particularly at certain scales, as fluid behavior begins to diverge from that in large-scale systems. This is especially notable in the slip flow regime, where the Knudsen (Kn) number falls between 0.001 and 0.1, highlighting the significance of solid surface–fluid interactions. In microchannels, these rarefaction effects cause fluid to experience slip flow, deviating from the classical no-slip boundary conditions observed in macroscale flows.

Numerical studies on microchannels are widely represented in the literature, with many exploring the behavior of fluids under various flow regimes and geometric configurations. For example, Türker & Öğüt (2022) examined the behavior of a hybrid nanofluid within a straight microchannel, varying the volumetric ratios of Al2O3 and CuO in a water-based fluid. By modifying these ratios, the changes in the Nusselt number, heat transfer coefficient, and pressure drop under different Reynolds numbers were analyzed, revealing the influence of the nanoparticle composition on microchannel flow. In another study, Shen et al. (2006) conducted experiments involving surface roughness within a heat sink consisting of 26 rectangular microchannels. Even though the flow was hydrodynamically developed, a decrease in the Nusselt number was observed for thermally developing flows, emphasizing how surface roughness influences thermal development. Further studies into the hydrodynamic entrance length of microchannels add to this body of knowledge. For example, Lobo & Chatterjee (2022) investigated the effect of sudden contraction due to fluid entering a microchannel from a plenum. By modifying the width

of the plenum at the channel inlet and outlet, they explored how this affected the hydrodynamic entrance length, particularly in the corner regions. They applied a no-slip boundary condition on solid surfaces and reported that the entrance length decreased within an aspect ratio range of 0.66-1.66 but could increase to a ratio of 20 beyond this range. They derived correlations for the entrance length as a function of both the Reynolds number and the aspect ratio. Similarly, Ferreira et al. (2021) developed correlations for the hydrodynamic entrance length by altering the aspect ratio from 0.1 to 1 and the Reynolds number from 0 to 2000. They emphasized the importance of predicting the entrance length precisely, especially when the Reynolds numbers are on the order of 1, because viscous forces prevail over inertial forces. Additionally, Ray & Das (2023) conducted 3D CFD simulations over Reynolds numbers ranging from 0.1-1000 and aspect ratios ranging from 0.125-1, deriving correlations for the hydrodynamic development length with respect to the Reynolds number. In exploring slip flow, Shaimi et al. (2023) considered slip flow on solid surfaces in microchannels, focusing on the thermal rather than the hydrodynamic entrance length. This analytical study highlighted how the Brinkman, Péclet, and Knudsen numbers affect the thermal entrance length, highlighting the importance of these dimensionless parameters in slip flow analysis. For accurate modeling of slip flow on surfaces, slip length models that incorporate Maxwell boundary conditions have been introduced in many studies (Wedel et al. (2022), Choi et al. (2003), Bhagat et al. 2019)). Djebali & Mokhtar (2022), for example, numerically investigated heat transfer and thermodynamic behavior in a Cu-water nanofluid microchannel under slip flow by using slip flow boundary conditions. This study recommends the use of microchannels for applications such as electronic cooling, emphasizing the role of the Knudsen number in flow dynamics. Similarly, Das and Tahmouresi (2016) analyzed slip flow in elliptical microchannels while considering different Reynolds numbers and characteristic lengths, revealing how microchannel geometry influences flow behavior. Silva & Semiao (2017) modeled low-speed gas flow within the slip flow regime, encompassing a wide Knudsen number range, and compared the results with those of the Navier–Stokes solutions. This study offers an innovative approach for gas flow modeling in microchannels, providing insights that might be extended to other areas of slip flow analysis. Avramenko et al. (2019) expanded upon these findings by examining slip boundary conditions and Knudsen number effects on velocity profiles in porous microchannels, assessing gas flow through porous structures under slip conditions. Zhang et al. (2020) used the Lattice Boltzmann method to explore slip flow in microchannels subjected to asymmetric heat fluxes, offering valuable engineering recommendations for optimizing heat transfer in microchannel systems. Micromachining processes may also impact surface characteristics, which, in turn, influence microchannel performance. Geng et al. (2023) investigated tool inclination during micromilling, focusing on surface roughness but without analyzing the flow structure. Kangude et al. (2024) evaluated how various tip clearance designs affect hydrodynamic performance and reported that appropriate designs can significantly enhance heat transfer. Harris et al. (2022) reviewed the effects of surface roughness, microstructures, and machining techniques, including milling, on microchannels and noted that different geometries and surface textures substantially impact heat transfer efficiency. In line with these findings, Bhandari et al. (2024) reported that machining methods such as milling significantly affect surface roughness, enhancing thermohydraulic performance by increasing heat transfer. Zhou et al. (2019) investigated copper microchannels fabricated via a multiblade milling process, which reduces wall roughness to optimize fluid flow, allowing efficient heat transfer. This study emphasizes the role of multibelade milling in enhancing surface smoothness, thereby improving heat transfer in high-performance applications such as electronic cooling. Xian (2019), in his doctoral thesis, examined how varying flow cross-sections within microchannels affect heat transfer, revealing that altering cross-sectional areas can reduce flow resistance and improve energy efficiency. Finally, Hou & Chen (2020) investigated pressure drop and heat transfer in microchannels with reentrant cavity geometries and reported that while these cavities increase the flow resistance and pressure drop, they also increase heat transfer, illustrating a trade-off in design choices.

When examining the focal points of the studies listed above, various parameters within the microchannel concept have been thoroughly investigated. The literature reveals that the effects of changes in channel diameter, cross-sectional area, and entrance length on hydrodynamic and thermal performance have been widely studied. Additionally, flow regimes characterized by dimensionless numbers such as Knudsen and Reynolds numbers have been emphasized in these studies, highlighting the significance of slip flow and rarefaction effects. Many studies have focused on the Maxwell slip model, particularly investigations of slip length at high Knudsen numbers. With respect to thermal performance, various studies have examined changes in the heat transfer coefficient and Nusselt number through the use of nanoparticles. Finally, the impact of machining techniques and surface roughness on hydrodynamic and thermal resistance has revealed how manufacturing-related differences can affect performance. While many studies explore these aspects, the influence of the tool's entry angle and the resulting geometric shape at the channel inlet or

outlet on microchannel performance has not been sufficiently addressed in the literature, which serves as the main motivation for this study. Furthermore, although some of the studies mentioned above focus on microchannel geometry and slip flow regimes, slip flow conditions have not always been considered. Although slip flow conditions are increasingly studied, the effects of inlet machining angles on microchannel efficiency, pressure drop, and overall performance are relatively underexplored, presenting an opportunity for further optimization of microchannel designs. With this in mind, this study investigates the hydrodynamic characteristics of flow within microchannels under slip flow conditions at various Knudsen values and low Reynolds numbers via CFD simulations, employing the Maxwell slip model with tool entry angles of 15°, 30°, and 45°.

MODEL SETUP

The study was conducted via the commercial software StarCCM+, which employs the finite volume method. The flow within the channel was modeled under two-dimensional, steady-state, laminar flow conditions and solved via a segregated flow solver. Air was used as the working fluid at a constant density of 1.18415 kg/m³ and a dynamic viscosity of 0.00001853 Pa.s. During the analysis, the mean free path could be directly defined within the software. By modifying this value, analyses were conducted at different Knudsen numbers. Changes in the Reynolds number were achieved by adjusting the inlet velocity. The Knudsen formula is presented in Equation (1), where λ is the mean free path and L_C is the characteristic length.

$$Kn = \frac{\lambda}{L_c} \tag{1}$$

Similarly, the Reynolds number is defined in Equation (2), where ρ is the fluid density, V_{in} is the velocity at the inlet of the straight part of the channel, L_c is the hydraulic diameter (taken as the channel width in this study), and μ is the dynamic viscosity:

$$Re = \frac{\rho . V_{in} . L_c}{\mu} \tag{2}$$

In all analyses, the channel width was kept constant at 50 μm. The channel length was modeled to be 10 times the width. The characteristic length used in the calculations of the Reynolds and Knudsen numbers was the channel width. The studies were conducted for Kn values of 0.1, 0.01, and 0.001 and for Re values ranging from 1 to 100. These conditions include the slip flow regime and cover the range where the Navier–Stokes equations with slip boundary conditions are applicable (Figure 1).

Fig. 1. Classification of flow regimes on the basis of the Knudsen number.

Therefore, the Maxwell slip model was used within the software. This model allows for a nonzero slip velocity, which is associated with molecular-level effects. The model is particularly suitable for examining flow characteristics in microchannels with low Reynolds and Knudsen numbers (Das & Tahmouresi (2016)). The momentum accommodation factor was kept at a value of 1 in all analyses. Owing to slip flow conditions, partial slip was applied instead of no slip on the upper and lower surfaces of the channel. At the channel inlet, a velocity boundary condition was applied, whereas at the outlet, an ambient pressure condition was applied. To examine the hydrodynamic effect of the channel inlet machining angle, which is the main motivation of this study, simulations were conducted at four different inlet angles of 0°, 15°, 30°, and 45° for all Kn and Re conditions. Considering that these angles could be due to manufacturing, the total lengths of all channels were kept equal to simulate the real scenario accurately. For channels with an inclined inlet, the length of the converging section was defined as 25 μm, which corresponds to half of the channel width, to ensure equal total channel lengths among all configurations.

GRID INDEPENDENCY AND VALIDATION

The computational grid created for the numerical solutions was designed to consist of two-dimensional quadrilateral cells. To ensure the solution's independence from the number of cells, the grid was refined, and its effect on the pressure drop within the channel was observed. Once the cell number at which this parameter stabilized was reached, approximately the same grid settings and cell count were used for other operating conditions and geometries. As shown in Figure 2, the pressure drop stabilized from approximately 40,000 cells onward; therefore, 40,000 cells were used in all the simulations.

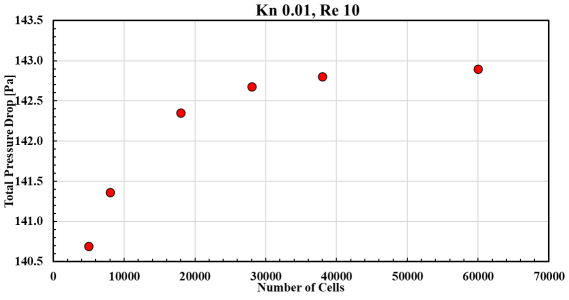

Fig. 2. Results of the grid independence study.

The final solution grids of the geometries with 0°, 15°, 30°, and 45° inlet machining angles are shown in Figure 3. Figure 4 presents a magnified view of the boundary layer mesh defined along the surface edges.

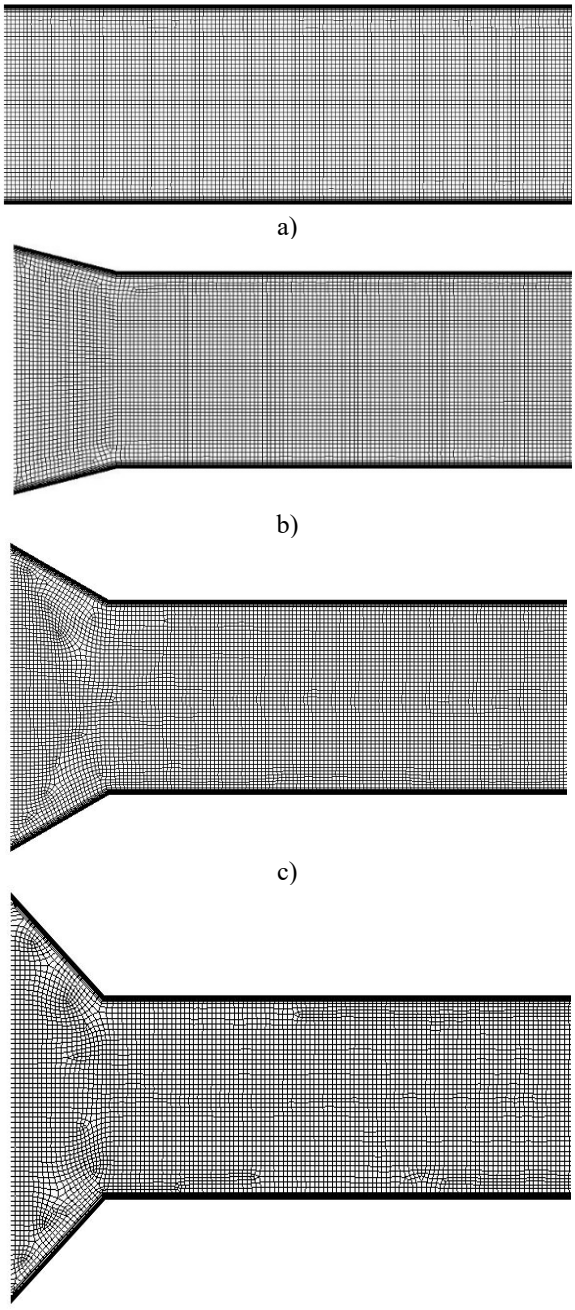

a) b) c) d)

Fig. 3. Final solution grid, a) 0°, b) 15°, c) 30°, and d) 45° inlet machining angles.

After concluding that the grid density and structure were sufficient, the obtained results were validated by comparing them with the analytical results provided by Karniadakis & Beskok (2005), as given in Equation (3). This equation provides the dimensionless velocity profile for fully developed flow conditions in microchannels. In this equation, b is a constant that can take values of 0, -1 or -2.

$$U^*(y,Kn) = \frac{-(y/h)^2 + y/h + Kn/(1-bKn)}{(1/6) + Kn/(1-bKn)} \quad (3)$$

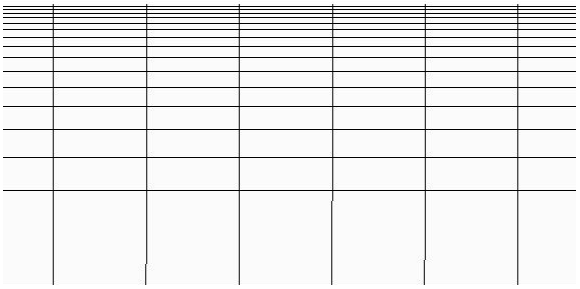

Fig. 4. Boundary layer mesh on the channel surface.

Figure 5 shows the dimensionless outlet velocity profile obtained from the simulation under Kn 0.01 and Re 10 conditions compared with the analytical results. Dimensionless scaling was achieved by dividing the outlet velocity profile by the average outlet velocity. As shown in Figure 5, the curves overlap with high accuracy. The consistency of the results with the analytical values on the channel surfaces defined with partial slip demonstrates the accuracy of the model. With these results confirming the validity of the method, the study proceeded accordingly.

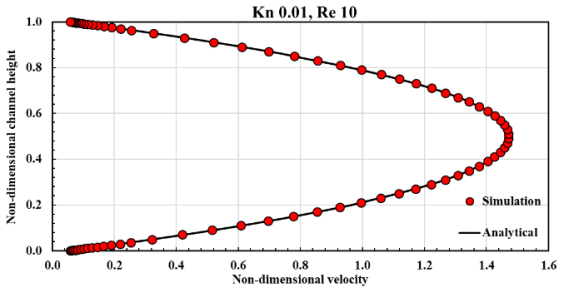

Fig. 5. Dimensionless outlet velocity profile.

RESULTS AND DISCUSSION

In the simulations conducted under Kn conditions of 0.1, 0.01, and 0.001 and for Re values ranging from 1 to 100, the pressure losses between the inlet and outlet of the channel were first calculated. The results are shown in Figure 6. As expected, with increasing Re, the velocity within the channel increases, leading to greater pressure losses. On the other hand, as Kn decreases, the pressure loss increases. For example, at Re 100 and a 45° inlet machining angle, the pressure loss at Kn 0.1, where slip flow is near the transition regime, is approximately 1300 Pa. This value increases to approximately 2300 Pa at a Kn of 0.001, where slip flow is closer to the continuum regime, representing a 75% increase. When the pressure loss ranking is examined on the basis of the inlet machining angle at a constant Re, it is observed that, as expected, the pressure loss decreases as the inlet machining angle

decreases. In percentage terms, the pressure loss relative to a straight channel increases by an average of 3% at a 15° inlet machining angle, 10% at a 30° inlet machining angle, and 25% at a 45° inlet machining angle across all Knudsen numbers. Additionally, for all three Knudsen numbers, as Re increases from 1 to 100, the pressure loss compared with that of the straight channel increases by approximately 8% for a 45° inlet machining angle. As the inlet machining angle decreases, this value gradually decreases to approximately 2% for a 15° inlet machining angle. These results indicate that during manufacturing, increasing the inlet machining angle to 45° can increase the pressure loss by up to 25%. Therefore, limiting the inlet angle to 30° is considered more appropriate, which results in a more reasonable pressure increase of approximately 10%.

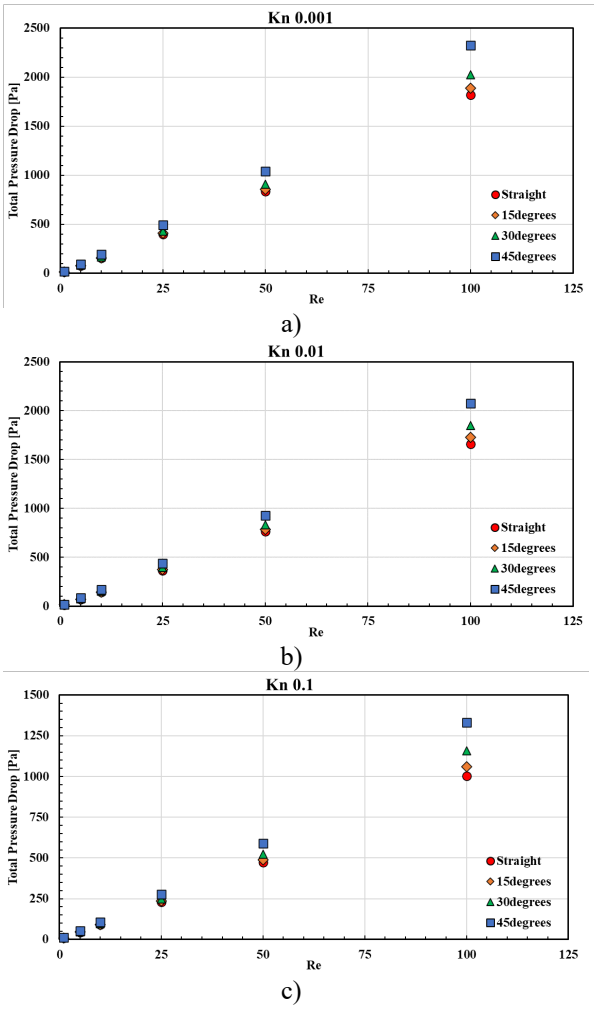

Fig. 6. Pressure drop within the channel for Kn values of a) 0.001, b) 0.01, and c) 0.1.

The observations and interpretations regarding the pressure drop are supported by the velocity contours shown in Figures 7 and 8. In the velocity contours provided for Kn 0.1 and Re 100 in Figure 7, as the machining inlet angle increases, a significant rise in velocity is observed in the convex corners due to the sudden contraction occurring in the inlet region of the channel. As the angle increases, the velocity rise in this section becomes more pronounced, which in turn increases the pressure drop. While this effect is slight at a 30° angle, it becomes highly prominent at 45°. Additionally, owing to the high Kn value near the transition region, the slip velocity along the solid surface edge reaches 12 m/s. On the other hand, similar contours for Re 100 are shown in Figure 8 for Kn 0.001, which is near the continuum regime. In this case, as the continuum regime approaches, the slip velocity nearly diminishes to zero. Consequently, the velocity difference between the channel center and the solid surface is greater than that at Kn = 0.1, with the high-velocity region around the center dominating a wider area from the channel inlet. This, in turn, leads to an increased pressure drop at lower Kn numbers.

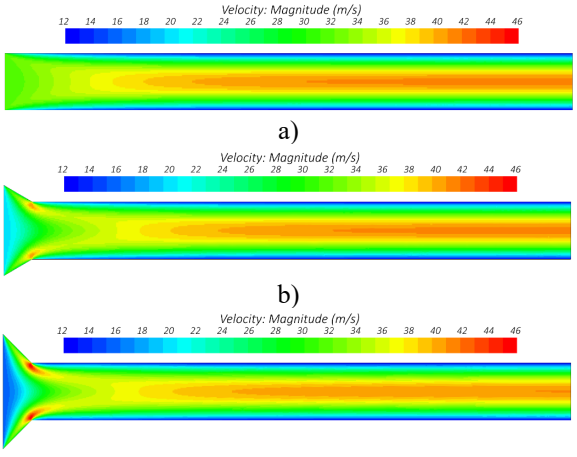

Fig. 7. Velocity contours for Kn 0.1 at Re 100: a) straight channel, b) 30° machining angle, and c) 45° machining angle.

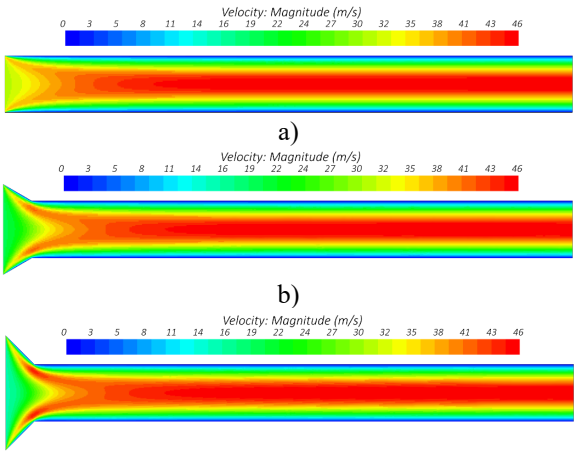

Fig. 8. Velocity contours for Kn 0.001 at Re 100: a) straight channel, b) 30° machining angle, and c) 45° machining angle.

Figures 9, 10, and 11 show the variation in the dimensionless velocity along the channel at the channel centerline, normalized by the velocity at the channel exit centerline. The channel direction on the horizontal axis is dimensionless and is normalized by the channel width. The results indicate that as the Reynolds number increases, the hydrodynamic entrance length increases. Similarly, at the same Reynolds number, as the Knudsen number increases (as it approaches the transition regime), this length also increases. However, the change due to the Knudsen effect is not as significant as the change due to the Reynolds number. Additionally, when the effect of the inlet angle for each Knudsen–Reynolds pair is analyzed, despite the different inlet widths due to varying inlet angles, the dimensionless velocity at the channel entrance is lower for larger inlet angles, as the boundary conditions are defined to maintain the same flow rate through the channel. However, unlike the differences in pressure loss, no change in the position where the velocity profile stabilizes (the hydrodynamic entrance length) is observed for any Knudsen–Reynolds pair after the development of the velocity profile. Although heat transfer is not included in this study, the stabilization of the velocity and temperature profiles independent of the inlet geometry, especially in long channels, could reduce the error in heat transfer and pressure loss calculations caused by the machining angle. However, as shown in Figures 9, 10, and 11, in cases where the channel length is on the order of the diameter for Re 1 or less than 7-8 times the diameter for Re 100, the inlet angle of the tool will directly affect the flow and potentially the heat transfer.

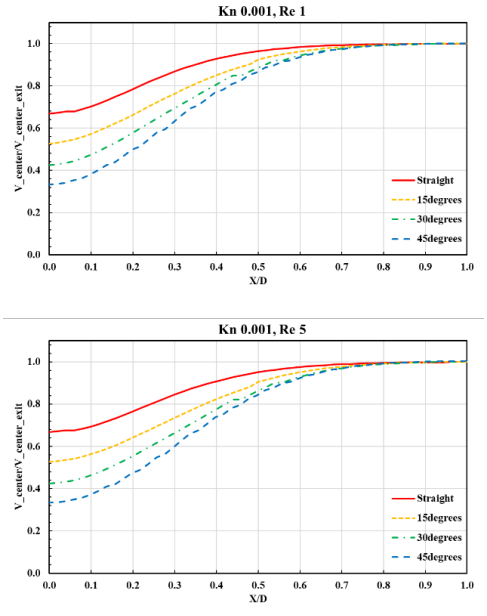

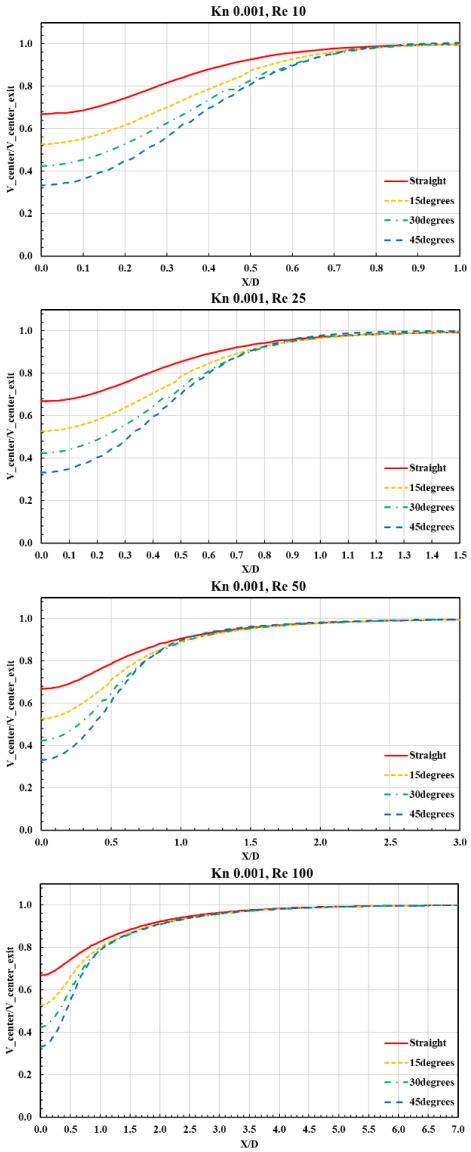

Fig. 9. Development of nondimensional centerline velocity along the flow direction at a Kn of 0.001.

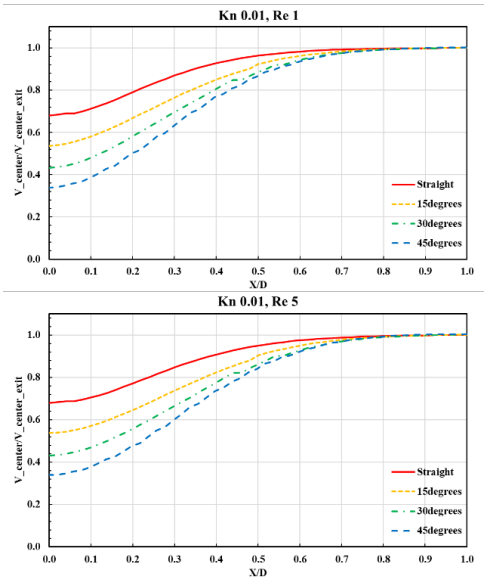

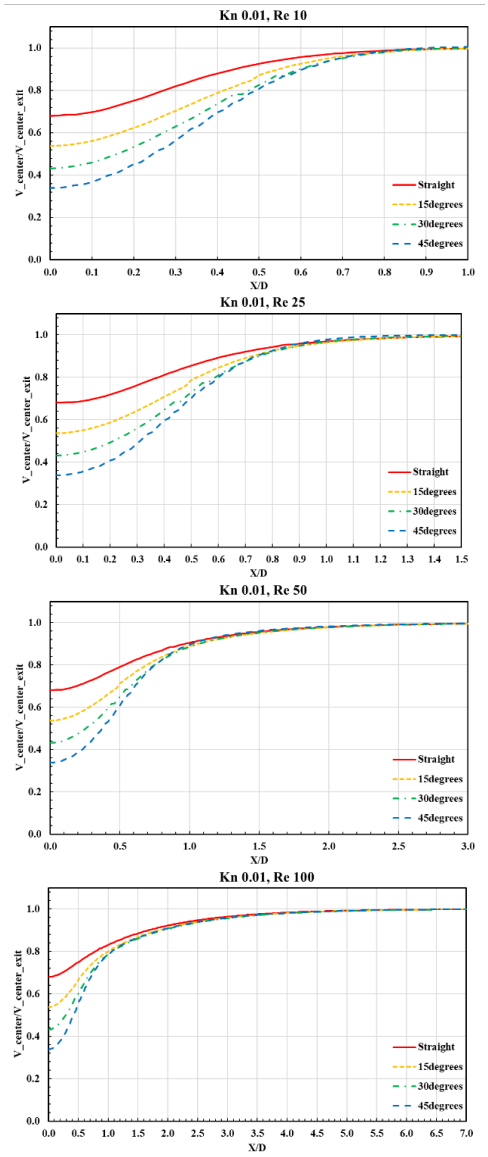

Fig. 10. Development of nondimensional centerline velocity along the flow direction at a Kn of 0.01.

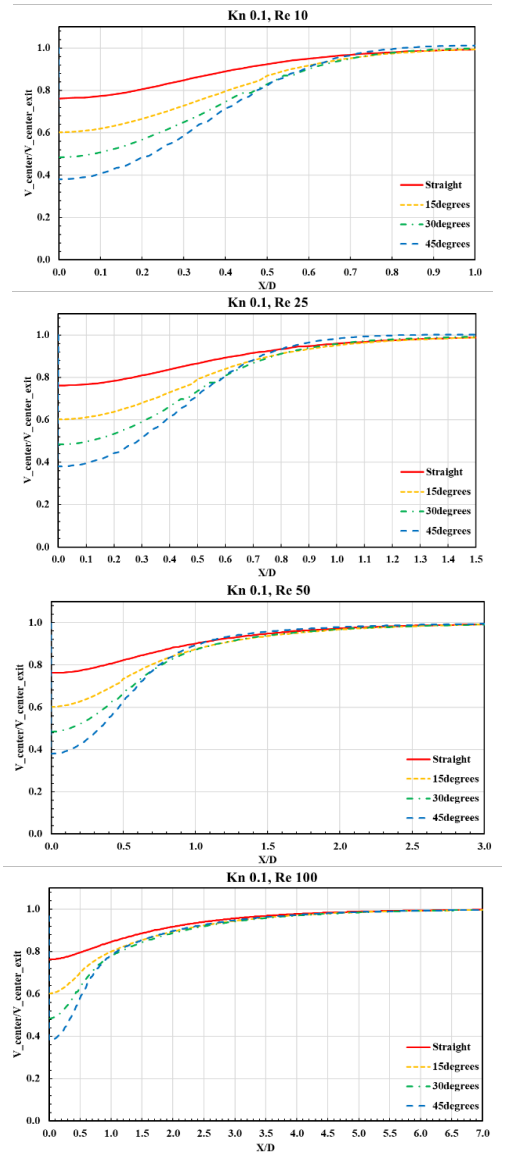

Fig. 11. Development of nondimensional centerline velocity along the flow direction at a Kn of 0.1.

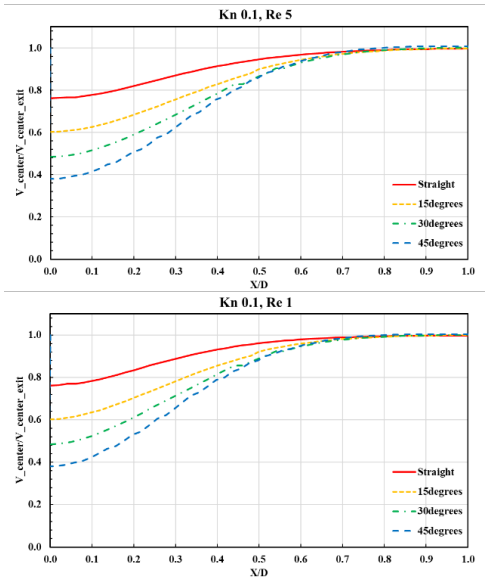

The nondimensional hydrodynamic entrance length values obtained for each Kn number are plotted as a function of the Re number and are presented in Figure 12. The results of this study have been compared with some findings in the literature, and the results are consistent. The equations from Chen (1973), Atkinson et al. (1969) and Ahmed & Hassan (2010), shown in the figure, are given solely as functions of the Re number. In the work conducted by the author of the present study with Aydın (Ilikan & Aydın (2023)), also presented in Figure 12, the effect of Kn is considered similar to that in the current study, where the Lattice-Boltzmann method was used instead of the Navier–Stokes solution. Figure 9-11 shows that while the machining inlet angle affects the channel pressure drop, it has no effect on the hydrodynamic entrance length. Therefore, while the values from the current study are

included in Figure 12, the inlet angle is not considered a parameter in that figure since the values obtained were the same for each inlet angle. On the other hand, it is observed from the graphs that the nondimensional hydrodynamic entrance length increases with the Re number and increases as the Kn number increases. In regions closer to the continuum regime (Kn 0.001 and Kn 0.01), the Lattice Boltzmann and Navier–Stokes solutions for each Kn almost overlap. However, for Kn 0.1, which is closer to the transition regime, there is a slight difference between the two solutions. Overall, the close agreement of the results within the Kn range considered demonstrates the validity of both methods within the Kn and Re ranges in this study. Based on the data obtained in the present study and shown in Figure 12, a correlation expressing the variation of hydrodynamic entrance length with Reynolds and Knudsen numbers has been developed and is presented in Equation (4).

$$\frac{L_e}{D_h} = \frac{0.735}{0.8058Re + 1} + Re^{0.67}(0.3832Kn^2 + 0.5833Kn + 0.2775) \quad (4)$$

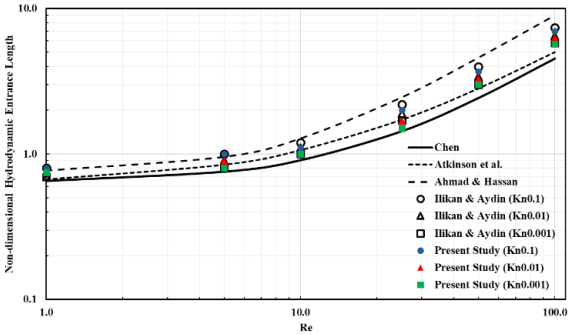

Fig. 12. Variations in the hydrodynamic entrance length with Re.

CONCLUSION

This study focused on the effects of the machining inlet angle on the pressure drop inside the microchannel and the hydrodynamic entrance length. Two-dimensional CFD simulations were performed by varying the Reynolds number from 1 to 100 under conditions where the Knudsen number was 0.001, 0.01, or 0.1. The findings can be summarized as follows:

-When the Kn number decreased from 0.1 to 0.001, the pressure drop increased by up to 75%, indicating that the Kn number plays a significant role in microchannel flow behavior.

-The machining inlet angle plays an important role in the flow pressure loss. At a 15° inlet angle, the pressure loss increased by an average of 3% compared with that of a straight inlet channel in the studied Re range. This value increased with the machining angle, reaching 25% at a 45° angle. This effect becomes more significant as the Re number increases, highlighting the importance of the interaction between the machining inlet angle and flow conditions.

-When the channel length is approximately equal to the diameter at Re 1 and less than 7-8 times the diameter at Re 100, the selection of the inlet machining angle is critical for reducing pressure losses. However, for longer channels, more flexibility in the selection of this angle is possible.

-In general, keeping the machining inlet angle below 30° may offer a practical balance between minimizing pressure losses and manufacturability, based on the trends observed in this study. This could lead to the development of more efficient microchannel-based systems. However, additional simulations with smaller angle increments could help refine this recommendation.

ACKNOWLEDGMENT

The author expresses sincere gratitude to the TÜBİTAK Rail Transport Technologies Institute (RUTE) for providing the infrastructure essential for this research.

REFERENCES

Ahmad, T., and Hassan, I., “Experimental Analysis of Microchannel Entrance Length Characteristics Using Microparticle Image Velocimetry,” *Journal of Fluids Engineering*, Vol.132, No.4, 041102,(2010).https://doi.org/10.1115/1.4001292

Atkinson, B., Brocklebank, M.P., Card, C.C.H., and Smith, J.M., “Low Reynolds Number Developing Flows,” *AIChE Journal*, Vol.15, No.1, pp. 548-553 (1969). https://doi.org/10.1002/aic.690150414

Avramenko, A.A., Kovetska, Y.Y., Shevchuk, I.V., and Tyrinov, A.I., “Heat Transfer in Porous Microchannels with Second Order Slipping Boundary Conditions,” *Transport in Porous Media*, Vol.129, No.1, pp. 673-699 (2019). https://doi.org/10.1007/s11242-019-01300-3

Bhagat, A., Gijare, H., and Dongar, N., “Modeling of Knudsen Layer Effects in the Micro-scale Backward-facing Step in the Slip Flow Regime,” *Micromachines*, Vol.10, No.2, pp. 118 (2019). https://doi.org/10.3390/mi10020118

Bhandari, P., Rawat, K.S., Prajapati, Y.K., Padalia, D. P., Ranakoti, L., and Singh, T., “A Review on Design Alteration in Microchannel Heat Sink for Augmented Thermohydraulic Performance,” *Ain*

Shams Engineering Journal, Vol.15, pp. 102417 (2024). https://doi.org/10.1016/j.asej.2023.102417

Chen, R.Y., "Flow in the Entrance Region at low Reynolds Numbers," *Journal of Fluids Engineering*, Vol.95, No.1, pp. 153-158 (1973). https://doi.org/10.1115/1.3446948

Choi, H., Lee, D., Maeng, J., "Computation of Slip Flow in Microchannels Using Langmuir Slip Condition," *Numerical Heat Transfer, Part A,* Vol.44, No.1, pp. 59-71 (2003). https://doi.org/10.1080/713838170

Das, S.K., and Tahmouresi, F., "Analytical Solution of Fully Developed Gaseous Slip Flow in Elliptic Microchannel," *International Journal of Advanced Applied Mathematics and Mechanics*, Vol.3, No.3, pp. 1-15. (2016).

Djebali, R., and Mokhtar, F., "Heat Transfer Appraising and Second Law Analysis of Cu-water Nanoliquid Filled Microchannel: Slip Flow Regime," *Romanian Journal of Physics*, Vol.67, No.605, pp. 1-25 (2022).

Ferreira, G., Sucena, A., and Ferrás, L.L., "Hydrodynamic Entrance Length for Laminar Flow in Microchannels with Rectangular Cross-section." *Fluids*, Vol.6, No.240, pp. 1-13. (2021). https://doi.org/10.3390/fluids6070240

Geng, Y., Zhang, S., Wang, J., Xiao, G., Li, C., and Yan, Y., "Effect of the Inclined Angle of Micromilling Tool on the Fabrication of the Microfluidic Channel," *The International Journal of Advanced Manufacturing Technology*, Vol.125, No.12, pp. 3069-3079 (2023).https://doi.org/10.21203/rs.3.rs-2373409/v1

Harris, M., Wu, H., Zhang, W., and Angelopoulou, A., "Overview of Recent Trends in Microchannels for Heat Transfer and Thermal Management Applications." *Chemical Engineering and Processing-Process Intensification*, Vol.181, pp. 109155(2022).https://doi.org/10.1016/j.cep.2022.109155

Hou, T., and Chen, Y., "Pressure Drop and Heat Transfer Performance of Microchannel Heat Exchanger with Different Reentrant Cavities," *Chemical Engineering & Processing: Process Intensification*, Vol.153, pp. 107931 (2020). https://doi.org/10.1016/j.cep.2020.107931

Ilikan, A.N., and Aydın, R., "Analysis of the Slip Flow in the Hydrodynamic Entrance Region of a 2D Microchannel." *Journal of Thermal Engineering*, Vol.9, No.3, pp. 733-745 (2023). https://doi.org/10.18186/thermal.1300390

Karniadakis, G., and Beskok, A., "Microflows and Nanoflows: Fundamentals and Simulation." *Springer*, Vol.1, pp. 254-268 (2005).

Kangude, P., Kumavat, P.S., Shatskiy, E., and Robinson, A.J., "Numerical Investigation of Tip Clearance Designs for Oblique-cut Fin Microchannels." *Applied Thermal Engineering*, Vol.257, pp. 124415 (2024). https://doi.org/10.1016/j.applthermaleng.2024.124415

Lobo, O.J., and Chatterjee, D., "Effect of Aspect Ratio on Entrance Length in Rectangular Plenum," *Physics of Fluids*, Vol.34, pp. 112009 (2022). https://doi.org/10.1063/5.0119897

Prakash, S., and Kumar, S., "Fabrication of Microchannels: A Review," *Proceedings of the Institution of Mechanical Engineers, Part B: Journal of Engineering Manufacture*, Vol.229, No.8, pp. 1273-1288 (2015). https://doi.org/10.1177/0954405414535581

Ray, D.R., and Das, D.K., "Simulations of Flows via CFD in Microchannels for Characterizing Entrance Region and Developing New Correlations for Hydrodynamic Entrance Length," *Micromachines*, Vol.14, No.7, pp 1418. (2023). https://doi.org/10.3390/mi14071418

Shaimi, M., Khatyr, R., and Naci, J.K., "Thermal Entrance Length for the Laminar Forced Convection in Microtubes," *Proceedings of the 9th World Congress on Mechanical, Chemical, and Material Engineering*. (2023).https://doi.org/10.11159/icmie23.152

Shen, S., Xu, J.L., Zhou, J.J., and Chen, Y., "Flow and Heat Transfer in Microchannels with Rough Wall Surface," *Energy Conversion and Management*, Vol.47, pp. 1311-1325 (2006). https://doi.org/10.1016/j.enconman.2005.09.001

Silva, G., and Semiao, V., "Consistent Lattice Boltzmann Modeling of Low-speed Isothermal Flows at Finite Knudsen Numbers in Slip-flow Regime: Application to Plane Boundaries," *Physical Review E*, Vol.96, pp. 013311 (2017). https://doi.org/10.1103/PhysRevE.96.013311

Türker, H., and Öğüt, E., "Investigation of Flow and Thermal Characteristics of Hybrid Nanofluid in a Straight Microchannel," *European Journal of Science and Technology*, Vol.36, pp. 255-261 (2022). https://doi.org/10.31590/ejosat.1112755

Wedel, J., Štrakl, M., Ravnik, J., and Stei, P., "A Specific Slip Length Model for the Maxwell Slip Boundary Conditions in the Navier–Stokes Solution of Flow Around a Microparticle in the No-slip and Slip Flow Regimes," *Theoretical Computational Fluid Dynamics*, Vol.36, pp. 723-740(2022).https://doi.org/10.1007/s00162-022-00627-w

Xian, C. K., "Convective Heat Transfer in Microchannels with Varying Flow Cross Section," *Nanyang Technological University*, Vol.1, pp. 98-105 (2019). https://doi.org/10.32657/10356/136773

Zhang, Y., Xie, G., and Karimipour, A., "Comprehensive Analysis on the Effect of Asymmetric Heat Fluxes on Microchannel Slip Flow and Heat Transfer via a Lattice Boltzmann Method," *International Communications in Heat and Mass Transfer*, Vol.118, pp. 104856 (2020). https://doi.org/10.1016/j.icheatmasstransfer.2020.104856

Zhou, F., Ling, W., Zhou, W., Qiu, Q., and Chu, X., "Heat Transfer Characteristics of Cu-based Microchannel Heat Exchanger Fabricated by Multiblade Milling Process," *International Journal of Thermal Sciences*, Vol.138, pp. 559-575(2019).https://doi.org/10.1016/j.ijthermalsci.2019.01.007

NOMENCLATURE

D	Channel height, [m]
Kn	Knudsen number, [-]
Lc	Characteristic length, [m]
μ	Dynamic viscosity, [Pa.s]
Re	Reynolds number, [-]
U*	Nondimensional velocity, [-]
x,y	Cartesian coordinates
V	Velocity, [m/s]
Vin	Inlet velocity, [m/s]
λ	Mean free path, [m]